

RL-Driven Sustainable Land-Use Allocation for the Lake Malawi Basin

Ying Yao

Georgia Institute of Technology

yyao374@gatech.edu

Abstract—Unsustainable land-use practices in ecologically sensitive regions threaten biodiversity, water resources, and the livelihoods of millions. This paper presents a deep reinforcement learning (RL) framework for optimizing land-use allocation in the Lake Malawi Basin to maximize total ecosystem service value (ESV). Drawing on the benefit transfer methodology of Costanza et al., we assign biome-specific ESV coefficients—locally anchored to a Malawi wetland valuation—to nine land-cover classes derived from Sentinel-2 imagery. The RL environment models a 50×50 cell grid at 500 m resolution, where a Proximal Policy Optimization (PPO) agent with action masking iteratively transfers land-use pixels between modifiable classes. The reward function combines per-cell ecological value with spatial coherence objectives: contiguity bonuses for ecologically connected land-use patches (forest, cropland, built area etc.) and buffer zone penalties for high-impact development adjacent to water bodies. We evaluate the framework across three scenarios: (i) pure ESV maximization, (ii) ESV with spatial reward shaping, and (iii) a regenerative agriculture policy scenario. Results demonstrate that the agent effectively learns to increase total ESV; that spatial reward shaping successfully steers allocations toward ecologically sound patterns, including homogeneous land-use clustering and slight forest consolidation near water bodies; and that the framework responds meaningfully to policy parameter changes, establishing its utility as a scenario-analysis tool for environmental planning.

Index Terms—reinforcement learning, ecosystem service value, land-use optimization, proximal policy optimization, Lake Malawi

I. INTRODUCTION

Lake Malawi, the third-largest lake in Africa, harbors extraordinary aquatic biodiversity—including more than 1,000 endemic cichlid fish species—and sustains the livelihoods of over five million people through fisheries, agriculture, and freshwater supply. Yet the basin faces accelerating pressures from deforestation, agricultural expansion, and unplanned urbanization, all of which degrade the ecosystem services on which local communities depend [1]. Making informed land-use decisions in such contexts requires a quantitative framework that can (i) value the diverse services provided by different biome types, (ii) account for spatial interactions among adjacent land parcels, and (iii) explore the consequences of alternative development strategies.

A. Ecosystem Service Valuation

The concept of ecosystem service value (ESV) provides a monetary accounting of the benefits that ecosystems deliver to human well-being, spanning provisioning services (food,

freshwater), regulating services (climate regulation, water purification), and cultural services (recreation, aesthetic value). Costanza et al. [2] pioneered the global estimation of these services at US\$33 trillion/yr (1995 dollars). A subsequent update using expanded valuation data from the Ecosystem Services Value Database (ESVD) [3] revised the estimate to US\$125 trillion/yr (2007 dollars) [4]. The underlying benefit transfer method assigns unit values (USD/ha/yr) to each biome type, making the trade-offs inherent in land-use decisions explicit: converting a wetland to cropland may increase provisioning output while sacrificing regulating services such as flood control and nutrient filtration [4]. This valuation framework forms the foundation for the reward function used in this study.

B. Deep Reinforcement Learning for Land-Use Optimization

Reinforcement learning (RL) formulates sequential decision-making as an agent interacting with an environment to maximize cumulative reward [5]. Recent advances in deep RL (DRL) have demonstrated the potential of this paradigm for spatial planning tasks. Zheng et al. [6] applied DRL with graph neural networks to urban community planning, optimizing land-use and road layouts to maximize the “15-minute city” accessibility metric. Shen et al. [7] proposed a DRL-based carbon emission mitigation strategy that integrates Points of Interest and transportation data to iteratively optimize urban land-use configurations. Later on, Shen et al. [8] extended this line of work to Hangzhou, using PPO to adjust cell-level land-use proportions and achieving up to 15% carbon emission reductions relative to baseline configurations.

A common pattern in these studies is to represent the study area as a grid, model cell-level land-use fractions as the RL state, and define actions as incremental transfers between land-use classes. Our work adopts a similar formulation but shifts the optimization target from carbon emission reduction in urban settings to ecosystem service value maximization in an ecological basin context—a setting with fundamentally different land-use classes (forest, wetland, rangeland) and conservation priorities (habitat connectivity, riparian buffer zones).

C. Contributions

This paper makes the following contributions:

- 1) A novel RL framework for ESV-driven land-use optimization in a non-urban, ecologically critical setting, the Lake Malawi Basin.
- 2) A multi-objective reward function that combines benefit-transfer ESV coefficients with spatial coherence terms—contiguity bonuses and water buffer penalties—grounded in ecological principles of habitat connectivity [9] and riparian protection [10].
- 3) An action masking mechanism that enforces physical constraints on land-use transfers, ensuring zero-sum conservation within each cell.
- 4) A systematic comparison of three policy scenarios that demonstrates the framework’s utility as an environmental planning and scenario analysis tool.

II. MATERIALS AND METHODS

A. Study Region

Lake Malawi is located between Malawi, Mozambique, and Tanzania and is the ninth-largest lake in the world by area. The study focuses on a $25\text{ km} \times 25\text{ km}$ area on the western shore of the lake, centered at latitude -13.934564° , longitude 34.542859° (Fig. 1). This region was selected for its diverse land-cover composition: water (12%), trees (20%), flooded/wetlands (24%), crops (4%), built area (20%), bare ground (12%), and rangeland (8%)—providing a rich testbed for multi-class land-use optimization.

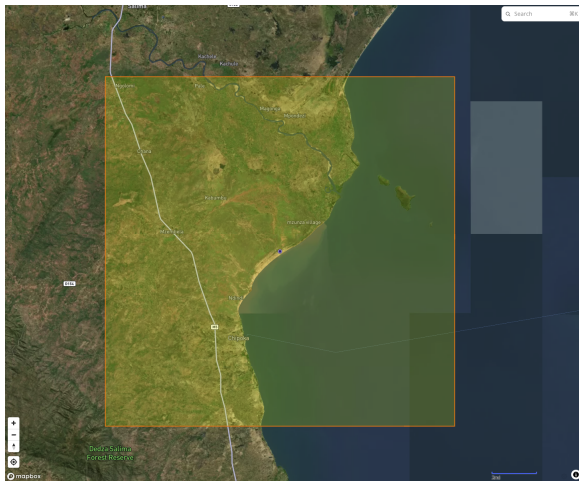


Fig. 1. Satellite view of the $25 \times 25\text{ km}$ study region on the western shore of Lake Malawi. The green overlay denotes the area of interest.

B. Data Sources and Preprocessing

1) *Land Cover*: Land-cover data were obtained from the ESA WorldCover product [11], derived from Sentinel-2 imagery at 10 m resolution for the year 2024. Nine land-cover classes are present in the study area (Table II). To reduce dimensionality, we downsample to 100 m resolution by taking the modal class within each 10×10 pixel block (10% sampling). The downsampled map is then organized into a grid of 50×50 cells, each cell comprising 5×5 pixels at 100 m, yielding

a 500 m effective resolution per cell. Each cell stores a 9-dimensional vector of pixel counts per land-cover class.

2) *Evapotranspiration*: Evapotranspiration (ET) data are drawn from the MODIS MOD16A3GF product [12] at 500 m resolution for 2024, accessed via the Planetary Computer API. Yearly ET values ($\text{kg}/\text{m}^2/\text{yr}$) are computed per land-cover class by area-weighted averaging over the study region (Table I). Trees exhibit the highest ET rate, consistent with their canopy transpiration, while bare ground and water surfaces sit at the lower end. While ET is not directly used in the reward function, it serves as an environmental constraint: episodes terminate early if the cumulative ET decrease exceeds a configurable tolerance, preventing allocations that would severely compromise water cycling.

TABLE I
PER-CLASS EVAPOTRANSPIRATION (2024, MOD16A3GF)

Class	Type	ET ($\text{kg}/\text{m}^2/\text{yr}$)
Water	Protected	616.93
Trees	Modifiable	933.57
Flooded	Protected	767.62
Crops	Modifiable	675.66
Built Area	Modifiable	648.95
Bare Ground	Modifiable	591.53
Snow/Ice	Protected	—
Clouds	Protected	845.87
Rangeland	Modifiable	745.94

C. Ecosystem Service Valuation

We adopt a benefit transfer approach to assign ESV coefficients to each land-cover class. Inter-biome ratios are derived from the updated unit values in Costanza et al. [4], which synthesizes over 300 case studies in the ESVD [3]. To anchor these global ratios to the local context, we calibrate against a primary valuation study for the Lake Chiuta wetland in southern Malawi, which estimated the gross financial value of inland wetland services at $\text{US}\$554/\text{ha}/\text{yr}$ [13]. Ratios for each biome type are then scaled relative to this anchor (Table II).

Four classes—water, flooded/wetlands, snow/ice, and clouds—are designated as *protected*: the RL agent can neither observe nor modify them, reflecting physical or regulatory constraints. The remaining five *modifiable* classes (trees, crops, built area, bare ground, rangeland) constitute the agent’s observation and action space.

All ESV coefficients are min-max normalized to $[0, 1]$ before use in the reward function, ensuring that no single class dominates the gradient signal by virtue of its absolute dollar value. Among the modifiable classes, the normalized values rank as: built area (0.26) > crops (0.22) > trees (0.21) > rangeland (0.16) > bare ground (0.00).

D. Training Dataset Preparation

The 50×50 cell grid is partitioned into non-overlapping 10×10 sub-patches, yielding 25 samples. These are split 70/30 into training and test sets, with indices fixed by a random seed. To mitigate overfitting on the small sample count, we apply

TABLE II
LAND-COVER CLASSES AND ECOSYSTEM SERVICE VALUES

Class	Type	ESV (USD/ha/yr)	Ratio
Water	Protected	554	1.00
Trees	Modifiable	238	0.43
Flooded	Protected	1,136	2.05
Crops	Modifiable	246	0.44
Built Area	Modifiable	295	0.53
Bare Ground	Modifiable	0	0.00
Snow/Ice	Protected	0	—
Clouds	Protected	0	—
Rangeland	Modifiable	184	0.33

spatial data augmentation: each original patch is randomly shifted by ± 2 cells in both row and column directions for $n_{\text{aug}} = 5$ rounds, expanding the effective training set by a factor of 6. Patches with a modifiable land fraction below 10% are rejected during episode initialization to ensure the agent has meaningful action opportunities.

E. Reinforcement Learning Framework

1) *State Space*: The observation at each timestep is a three-dimensional tensor $\mathbf{s} \in [0, 1]^{M \times M \times K}$, where $M = 10$ is the grid dimension and $K = 5$ is the number of modifiable land-cover classes. Each element $s_{i,j,k}$ represents the fraction of cell (i, j) occupied by modifiable class k , computed as the pixel count divided by the total pixels per cell ($N_p = 25$). Protected classes are excluded from the observation entirely (i.e., the agent has no channel for water or wetlands), however, the protected water fraction is retained internally for computing the buffer zone penalty.

2) *Action Space and Masking*: Each action is a 4-tuple $a = (i, j, c_{\text{src}}, c_{\text{tgt}})$, implemented as a `MultiDiscrete`[M, M, K, K] space. An action selects cell (i, j) and transfers $\Delta = 5$ pixels from source class c_{src} to target class c_{tgt} . The transfer is clamped so that the source fraction cannot fall below 0 and the target fraction cannot exceed 1, guaranteeing zero-sum conservation within each cell by construction. When $c_{\text{src}} = c_{\text{tgt}}$, or when the source class has zero pixels in the selected cell, the action is defined as a *no-op*.

To prevent the agent from wasting exploration on globally infeasible actions, we employ action masking via `MaskablePPO` [14], [15]. At each step, a boolean mask is computed per action dimension:

- **Row / Column**: all positions are valid (mask = all true).
- **Source**: class k is valid iff $\exists (i, j)$ such that $s_{i,j,k} > 0$.
- **Target**: class k is valid iff $\exists (i, j)$ such that $s_{i,j,k} < 1$.

This grid-level masking eliminates globally impossible transfers while keeping the mask computation $O(M^2K)$.

3) *Reward Function*: The reward at step t is the change in total value:

$$r_t = \frac{V(\mathbf{s}_{t+1}) - V(\mathbf{s}_t)}{\sigma} \quad (1)$$

where σ is a configurable reward scale and the total value V is defined as:

$$V(\mathbf{s}) = V_{\text{eco}}(\mathbf{s}) + \lambda_s \cdot V_{\text{spatial}}(\mathbf{s}) \quad (2)$$

The **ecological value** is the sum of ESV-weighted fractions across all cells:

$$V_{\text{eco}}(\mathbf{s}) = \sum_{i=1}^M \sum_{j=1}^M \sum_{k=1}^K s_{i,j,k} \tilde{e}_k \quad (3)$$

where \tilde{e}_k is the min-max normalized ESV coefficient for modifiable class k .

The **spatial value** captures landscape-level ecological coherence:

$$V_{\text{spatial}}(\mathbf{s}) = w_T C_T + w_C C_C + w_B C_B - w_W P_W \quad (4)$$

where C_T, C_C, C_B are contiguity scores for trees, crops, and built area respectively, and P_W is the water buffer penalty. Each contiguity score measures how much a given class is spatially clustered:

$$C_c = \ln\left(1 + \sum_{i,j} s_{i,j,c} (\mathbf{K} * \mathbf{s}_{:, :, c})_{i,j}\right) \quad (5)$$

Here \mathbf{K} is the 4-connected neighbor kernel $\begin{bmatrix} 0 & 1 & 0 \\ 1 & 0 & 1 \\ 0 & 1 & 0 \end{bmatrix}$ and $*$ denotes 2D convolution with zero-padded boundaries. The $\ln(1 + \cdot)$ transformation compresses the range to prevent large contiguous patches from dominating the reward signal.

The **buffer zone penalty** discourages high-impact land use (crops and built area) adjacent to water bodies:

$$P_W = \ln\left(1 + \sum_{i,j} (s_{i,j,\text{crop}} + s_{i,j,\text{built}}) (\mathbf{K} * \mathbf{w})_{i,j}\right) \quad (6)$$

where $\mathbf{w} \in [0, 1]^{M \times M}$ is the protected water fraction map (water + flooded classes). This term penalizes the agent for placing crops or built area in cells whose neighbors contain water, encoding the ecological principle that riparian buffer zones reduce nutrient runoff and protect aquatic ecosystems [10].

4) *Termination Conditions*: An episode terminates when any of the following conditions is met:

- 1) **Step limit**: the agent has taken $T_{\text{max}} = 500$ steps.
- 2) **ET constraint**: the fractional decrease in total evapotranspiration from the initial state exceeds a tolerance $\tau_{\text{ET}} = 1.0$ (i.e., ET may decrease by up to 100%).
- 3) **Stagnation**: the agent has produced $n_{\text{noop}} = 10$ consecutive no-op actions, indicating it can find no further improving transfers.

The no-op termination condition is critical: it allows the agent to *choose* to stop early and spend more time on exploration rather than exploitation.

F. Network Architecture

We employ a custom CNN feature extractor (`GRIDCNN`) that replaces the default MLP feature extractor in `Stable-Baselines3`. The architecture processes the $K \times M \times M$ observation (channels first) as follows:

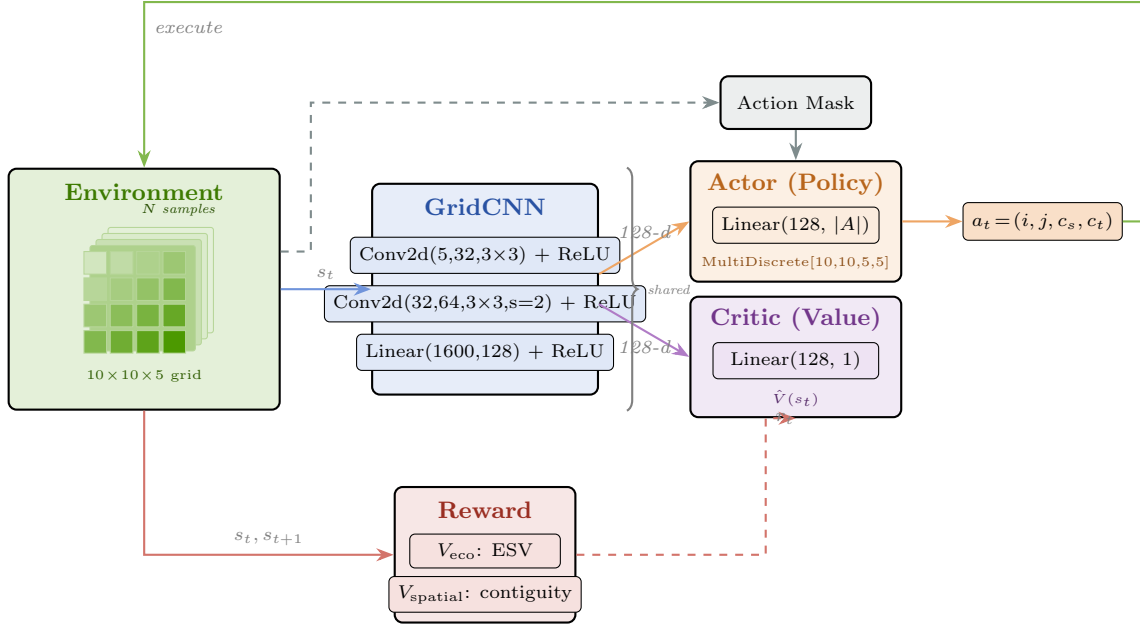


Fig. 2. Overview of the proposed RL framework. The agent observes a $10 \times 10 \times 5$ land-use fraction grid, extracts spatial features via a shared GridCNN, and produces both a masked policy (Actor) and state value estimate (Critic). The environment executes the selected action and returns a reward combining ESV change and spatial coherence metrics.

- 1) Conv2d($K=5$, 32, 3×3 , stride = 1, pad = 1) \rightarrow ReLU
- 2) Conv2d(32, 64, 3×3 , stride = 2, pad = 1) \rightarrow ReLU
- 3) Flatten \rightarrow Linear(1600, 128) \rightarrow ReLU

The first convolutional layer preserves the 10×10 spatial dimensions with a 3×3 receptive field—structurally aligned with the 4-connected contiguity kernel \mathbf{K} used in the reward function. This inductive bias allows the network to directly learn representations of local neighbor relationships relevant to the spatial reward terms. The second layer, with stride 2, reduces the spatial dimensions to 5×5 and captures multi-cell cluster patterns. The resulting 128-dimensional feature vector is shared between the actor and critic heads of the PPO agent.

G. Training Configuration

The agent is trained using MaskablePPO [14], [16] from the SB3-Contrib library [15]. Table III lists the hyperparameters used across all experiments. Training runs for 500,000 timesteps with metrics logged to Weights & Biases.

III. RESULTS

We evaluate the framework across three experimental scenarios that progressively add complexity to the reward signal. In each experiment, the trained agent is evaluated on both training and test patches; the resulting cell-level allocations are reconstructed onto the full 50×50 grid and visualized as side-by-side before/after heatmaps. Each cell displays horizontal bars representing land-use type fractions, and the background color encodes the cell’s total ecosystem value (red = high, white = low). Black-bordered cells indicate locations modified by the agent.

TABLE III
PPO HYPERPARAMETERS

Parameter	Value
Learning rate	1×10^{-4}
Rollout length (n_{steps})	2,048
Mini-batch size	128
PPO epochs	10
Discount (γ)	0.99
GAE λ	0.95
Clip range	0.2
Entropy coefficient	0.02
Value function coeff.	0.5
Max gradient norm	0.5
Total timesteps	500,000

A. Experiment I: ESV Maximization ($\lambda_s = 0$)

In this baseline experiment, the spatial reward scale is set to zero ($\lambda_s = 0$), so the agent optimizes purely for per-cell ecological value (Eq. 3). Because built area has the highest normalized ESV among modifiable classes (0.26), the rational greedy strategy is to convert low-value classes (bare ground, rangeland) toward built area.

Fig. 3 confirms this expectation: the agent aggressively expands built area across the grid. Bare ground and rangeland fractions decrease substantially, replaced predominantly by built area, with some increase in crops (the second-highest value class at 0.22). The “after” map shows a pronounced reddening across the inland portion of the grid, indicating higher cell-level ESV but at the cost of ecological realism—the resulting allocation resembles unconstrained urban sprawl rather than sustainable land management.

This result validates that the RL agent *is* learning to maximize its reward, but simultaneously reveals the insufficiency of a purely value-based objective: without spatial constraints, the agent exploits the reward function in ways that are ecologically undesirable.

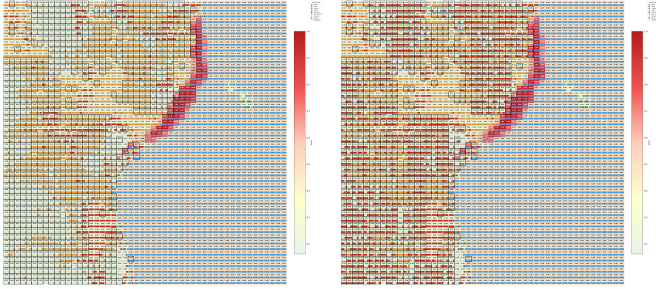


Fig. 3. Exp I results ($\lambda_s = 0$). Left: initial land-use allocation. Right: allocation after agent optimization.

B. Experiment II: Spatial-Ecological Optimization ($\lambda_s = 1$)

This experiment activates the full spatial reward (Eq. 4) with weights $w_T=1$, $w_C=3$, $w_B=3$, $w_W=5$ (Table IV). The tree contiguity weight is set lower than crop and built contiguity because trees already have a moderate base ESV; the higher crop and built weights encourage consolidation of these classes into contiguous blocks rather than scattering them. The water buffer penalty receives the highest weight, reflecting the ecological priority of protecting riparian zones.

TABLE IV
SPATIAL REWARD WEIGHTS

Component	Symbol	Weight
Tree contiguity bonus	w_T	1.0
Crop contiguity bonus	w_C	3.0
Built-area contiguity bonus	w_B	3.0
Water buffer penalty	w_W	5.0

Fig. 4 shows markedly different behavior compared to Exp I. The agent produces more nuanced allocations with several notable patterns:

- **Forest consolidation:** tree fractions increase in areas adjacent to existing forest patches, forming more contiguous canopy cover rather than scattered fragments.
- **Built-area clustering:** urban expansion still occurs but is more spatially concentrated, reflecting the built contiguity bonus rather than uniform sprawl.
- **Water protection:** cells adjacent to the lake and wetland boundaries are shown only slight transfer from built-area/crop to trees though, which may be further optimized by calibrating the weight.

The overall ESV increase is smaller than in Exp I because the spatial penalties constrain some high-value-per-cell conversions, but the resulting landscape is more ecologically coherent.

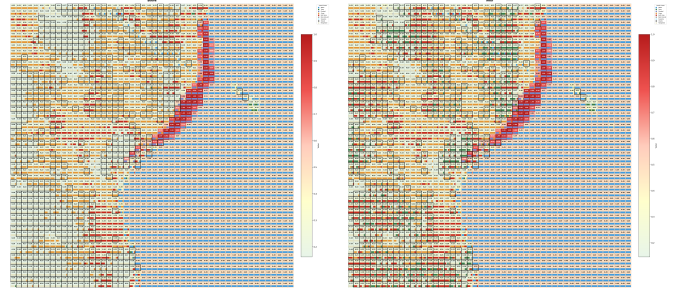


Fig. 4. Exp II results ($\lambda_s = 1$, spatial rewards active).

C. Experiment III: Regenerative Agriculture Scenario

This experiment uses **identical spatial reward** weights as Exp II but increases the crop ESV coefficient by 35% (from \$246 to \$332/ha/yr), simulating a policy scenario in which regenerative agricultural practices (e.g., agroforestry, cover cropping) enhance the ecosystem service output of cropland. After re-normalization, the crop class (0.29) now exceeds built area (0.26) as the highest-value modifiable class.

Fig. 5 shows a visible shift toward agricultural allocation compared to Exp II. The agent converts more bare ground and rangeland to crops rather than built area, and cropland patches appear more contiguous—driven by both the higher per-cell crop value and the crop contiguity bonus ($w_C = 3$). Built-area expansion is relatively restrained, demonstrating that the framework is sensitive to policy-driven changes in ESV coefficients.

This result illustrates the framework’s potential as a **scenario analysis tool**: by adjusting ESV coefficients, stakeholders can explore how different agricultural policies, conservation incentives, or development regulations would alter optimal land-use patterns. The RL agent serves as an optimizer that translates these value assumptions into concrete spatial allocations.

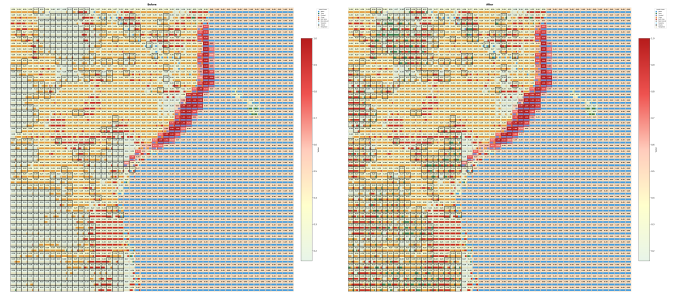


Fig. 5. Exp III results (regenerative agriculture scenario). With crop ESV increased by 35%, the agent shifts allocation preference from built area toward cropland, demonstrating policy sensitivity.

D. Zoom-In Comparison Across Experiments

To further demonstrate the experiment results above and make the per-cell allocation drift across the three experiments legible, Fig. 6 pairs an overview of the original allocation with a 4×3 zoom grid: rows correspond to the original state and

each of the three experiments, while columns correspond to three 5×5 -cell example regions (outlined on the overview in matching colours). All panels share a single ESV colormap so cell-level value shifts are directly comparable. The black borders inside each panel mark cells modified by the agent in that experiment, matching the convention of Figs. 3–5.

E. Metric Analysis and Result Comparison

Beyond the qualitative side-by-side maps, we examine the training diagnostics logged to Weights & Biases to verify that the agent’s learned behavior reflects genuine convergence rather than an artifact of reward scaling or update-step instability. Unless otherwise stated, all metrics refer to the spatially-aware scenarios (Exp II and III), which are trained under the richer reward signal and are the primary object of analysis.

1) *Return and episode length*: The mean episode return (rollout/ep_rew_mean) rises from approximately 1–2 to 6–7 within the first $\sim 2.5k$ rollout steps and then plateaus for the remainder of training, with a few stochastic fluctuations on top (Fig. 7, left). Mean episode length settles around 200–250 steps, well below the $T_{\max} = 500$ cap, confirming that the no-op termination condition is the dominant stopping criterion.

2) *Critic fit and loss curves*: The value function converges rapidly: train/explained_variance rises to ≈ 0.9 within the first few thousand steps and holds steady, and train/value_loss decays to a low, stable floor (Fig. 8). Combined with the plateaued return, these curves show that the critic has accurately fit the state-value landscape and that further training produces no systematic improvement in performance.

The policy-gradient loss (train/pg_loss) continues to drift slightly more negative throughout training. Since the quantity logged is the negated PPO surrogate objective, this indicates a continuous advantage obtained for action chosen based on new policy.

3) *Spatial reward components*: Fig. 9 breaks spatial rewards into its four sub-terms. Tree and built-area contiguity rewards climb slowly but steadily in both Exp II and III, confirming that the agent is gradually consolidating forest and urban cells into larger contiguous blocks. The crop contiguity reward is the clearest difference between the two scenarios: under Exp II it hovers around a small negative mean, whereas in Exp III the regenerative-agriculture multiplier pulls it into a small positive range, showing that a higher crop ESV directly translates into more clustered cropland allocations. The water buffer penalty stays two orders of magnitude smaller than the other three components throughout training, which explains the modest riparian protection observed in Fig. 4 and suggests that w_W needs to be recalibrated upward to exert a meaningful influence on the policy.

4) *Summary*: Table V summarizes the qualitative behavioral differences across the three experiments. Combined with the quantitative training diagnostics above, the progression from Exp I to III demonstrates four key findings: (1) the RL agent reliably learns to maximize its reward signal, with return converging within the first $\sim 10\%$ of training; (2) the critic

fully fits the state-value landscape (explained variance ≈ 0.9); (3) spatial reward shaping is effective at steering allocations toward ecologically desirable patterns without requiring hard constraints; and (4) the framework responds meaningfully to changes in ESV coefficients, confirming its utility for policy scenario analysis.

TABLE V
BEHAVIORAL COMPARISON ACROSS EXPERIMENTS

	Exp. I (Eco only)	Exp. II (+ Spatial)	Exp. III (+ Regen. Ag.)
Spatial scale	$\lambda_s=0$	$\lambda_s=1$	$\lambda_s=1$
Dominant conversion	→ Built	Mixed	→ Crops
Forest near water	Not Obvious	Slightly Increased	Slightly Increased
Built expansion	Aggressive	Clustered	Clustered + Restrained
Crop allocation	Moderate	Moderate	High
Ecological realism	Low	High	High

IV. DISCUSSION AND CONCLUSION

A. Discussion

The experimental results confirm that deep reinforcement learning can serve as an effective mechanism for land-use allocation optimization when grounded in a well-designed reward function. Several aspects merit further discussion.

Reward design as policy encoding. The transition from Exp I to Exp II illustrates that reward shaping is not merely a training aid but a form of *policy encoding*. The contiguity bonuses and buffer penalties translate ecological principles—habitat connectivity [9] and riparian protection [10]—into differentiable objectives that the agent can optimize through gradient-based learning. This approach is more flexible than hard constraints because the weights can be tuned to reflect varying policy priorities without modifying the environment logic.

CNN inductive bias. The GridCNN feature extractor’s 3×3 convolutional filters are structurally aligned with the 3×3 contiguity kernel used in the spatial reward computation. This architectural choice provides an inductive bias that helps the actor and critic networks learn representations of local spatial patterns relevant to the reward. While the small grid size (10×10) means an MLP could potentially learn these relationships given sufficient data, the CNN provides a useful prior that may accelerate learning and improve sample efficiency—though a formal ablation study is needed to quantify this benefit.

Policy scenario analysis. Exp III demonstrates a practical use case: a policymaker can adjust ESV coefficients to simulate “what-if” scenarios (e.g., subsidizing regenerative agriculture) and observe how optimal land-use allocations shift. The RL agent acts as an optimizer that translates value assumptions into spatial strategies, providing a computational complement to traditional cost-benefit analysis.

Original land-use allocation (zoom regions outlined)

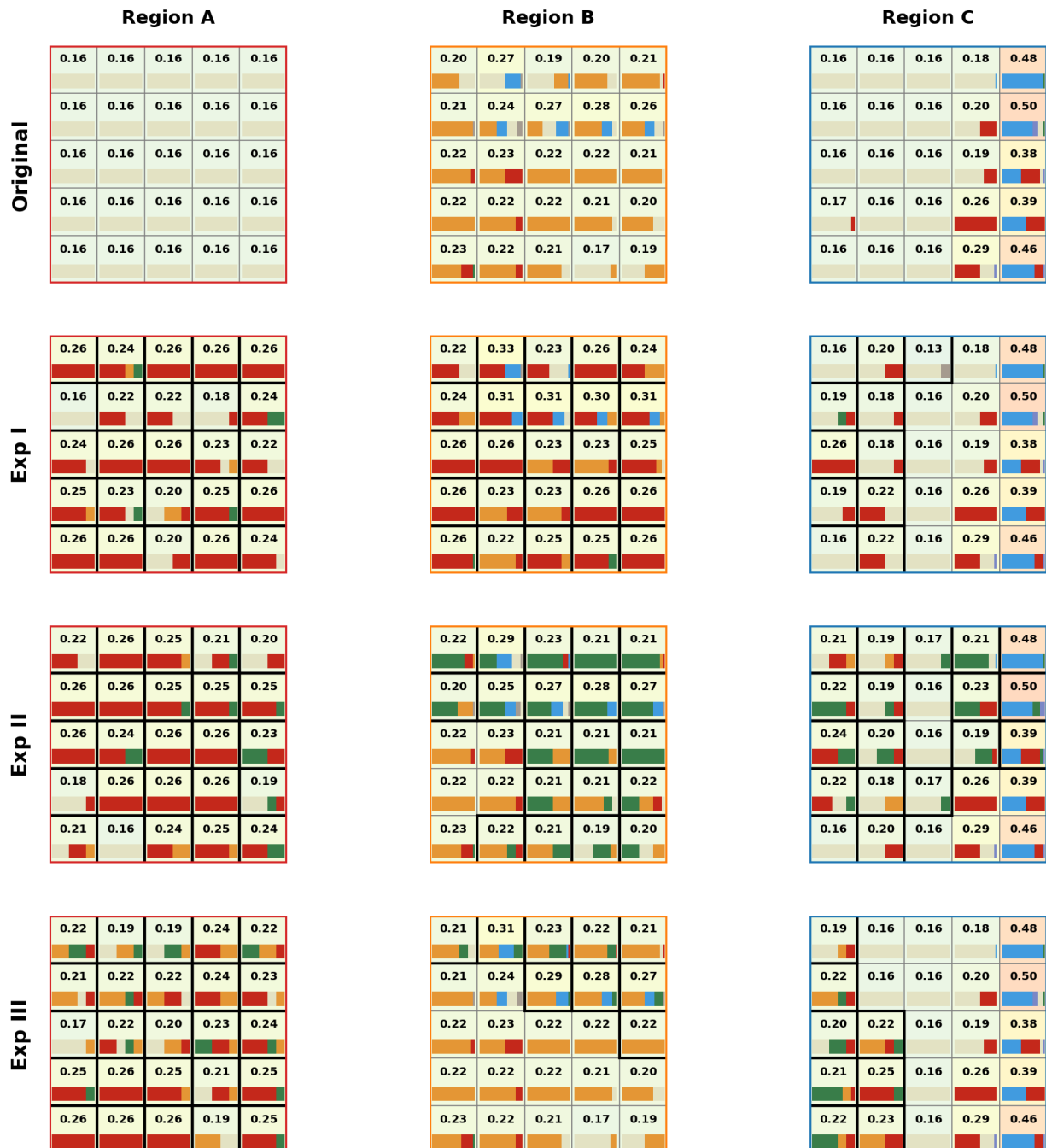
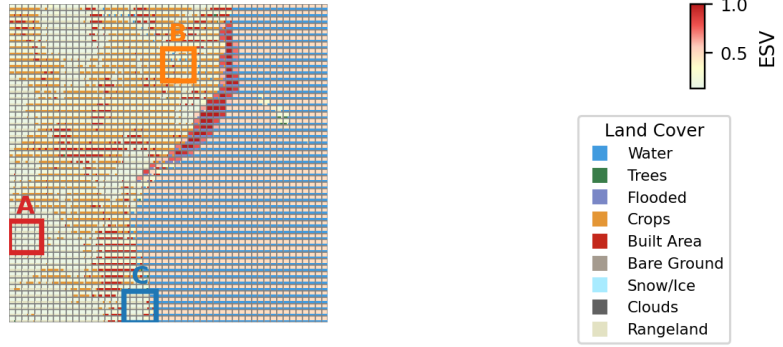


Fig. 6. Zoom-in comparison across experiments. **Top:** original land-use allocation with three coloured boxes marking the zoom regions. **Bottom:** per-region zooms for the original allocation and the final allocation of each experiment.

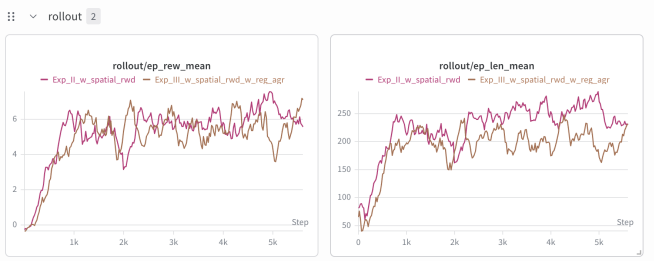


Fig. 7. Training return (left) and episode length (right).

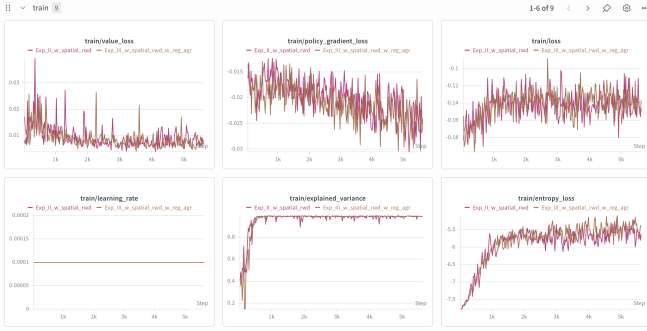


Fig. 8. Training losses and diagnostics.



Fig. 9. Spatial reward components during training.

B. Limitations

The current study has several limitations that should be acknowledged:

- **No baseline comparison:** the current evaluation lacks comparison with alternative optimization methods (e.g., genetic algorithms, integer linear programming) that would contextualize the RL framework’s relative performance.
- **Single study region:** results are demonstrated on one geographic area; generalization to other areas with different land-cover distributions remains to be validated.
- **Static ESV coefficients:** the benefit-transfer values are fixed and do not account for nonlinear interactions between services, diminishing marginal returns, or temporal dynamics of ecosystem recovery.
- **Action masking granularity:** the source/target masks operate at the grid level (checking if *any* cell has the

class available) rather than at the cell level due to MaskablePPO’s property, meaning some selected actions may still resolve to no-ops at the cell level. Finer-grained masking could improve sample efficiency.

- **Reward-component balance across scenarios:** the spatial reward weights (w_T, w_C, w_B, w_W) are held fixed across the three experiments, but Exp III scales the crop ESV by 35% without re-scaling w_C . More study is preferred to estimate the impact and whether auto-calibration is needed.

C. Future Work

Several directions are worth pursuing: (i) conducting formal ablation studies on the GridCNN versus MLP feature extractor and on individual spatial reward components; (ii) scaling the framework to larger grids with hierarchical RL or attention-based architectures; (iii) benchmarking against established optimization baselines; and (iv) generalizing the framework to other ecologically sensitive regions beyond Lake Malawi to validate its transferability across diverse land-cover distributions and policy contexts.

D. Conclusion

This paper presented a reinforcement learning framework for optimizing land-use allocation in the Lake Malawi Basin to maximize ecosystem service value. By combining benefit-transfer ESV coefficients with spatial coherence rewards, the framework produces ecologically informed land-use plans that balance per-cell value maximization with landscape-level objectives. The three experimental scenarios demonstrate that the RL agent reliably learns to exploit its reward signal, that spatial reward shaping effectively encodes ecological principles into the optimization process, and that the framework is responsive to policy parameter changes. While significant work remains to scale the approach and validate it against baselines, the results establish a promising proof of concept for AI-assisted environmental planning in critical ecosystems.

REFERENCES

- [1] Millennium Ecosystem Assessment, *Ecosystems and Human Well-Being: Synthesis*. Washington, DC: Island Press, 2005.
- [2] R. Costanza, R. d’Arge, R. de Groot, S. Farber, M. Grasso, B. Hannon, K. Limburg, S. Naeem, R. V. O’Neill, J. Paruelo, R. G. Raskin, P. Sutton, and M. van den Belt, “The value of the world’s ecosystem services and natural capital,” *Nature*, vol. 387, pp. 253–260, 1997.
- [3] R. de Groot, L. Brander, S. van der Ploeg, R. Costanza, F. Bernard, L. Braat, M. Christie, N. Crossman, A. Ghermandi, L. Hein *et al.*, “Global estimates of the value of ecosystems and their services in monetary units,” *Ecosystem Services*, vol. 1, no. 1, pp. 50–61, 2012.
- [4] R. Costanza, R. de Groot, P. Sutton, S. van der Ploeg, S. J. Anderson, I. Kubiszewski, S. Farber, and R. K. Turner, “Changes in the global value of ecosystem services,” *Global Environmental Change*, vol. 26, pp. 152–158, 2014.
- [5] R. S. Sutton and A. G. Barto, *Reinforcement Learning: An Introduction*, 2nd ed. MIT Press, 2018.
- [6] Y. Zheng, Y. Lin, L. Zhao, T. Wu, D. Jin, and Y. Li, “Spatial planning of urban communities via deep reinforcement learning,” *Nature Computational Science*, vol. 3, no. 9, pp. 748–762, 2023.
- [7] J. Shen, F. Zheng, Y. Ma, W. Deng, and Z. Zhang, “Urban travel carbon emission mitigation approach using deep reinforcement learning,” *Scientific Reports*, vol. 14, no. 1, p. 27778, 2024.

- [8] J. Shen, F. Zheng, T. Chen, W. Deng, A. Bellotti, F. B. Tesema, and E. Lucchi, "Optimizing urban land-use through deep reinforcement learning: A case study in Hangzhou for reducing carbon emissions," *Land*, vol. 14, no. 12, 2025.
- [9] L. Fahrig, "Effects of habitat fragmentation on biodiversity," *Annual Review of Ecology, Evolution, and Systematics*, vol. 34, pp. 487–515, 2003.
- [10] R. Lowrance, R. Todd, J. Fail, O. Hendrickson, R. Leonard, and L. Asmussen, "Riparian forests as nutrient filters in agricultural watersheds," *BioScience*, vol. 34, no. 6, pp. 374–377, 1984.
- [11] D. Zanaga, R. Van De Kerchove, D. Daels, W. De Keersmaecker, C. Brockmann, G. Kirches, J. Wevers, O. Cartus, M. Santoro, S. Fritz *et al.*, "ESA WorldCover 10 m 2021 v200," *Zenodo*, 2022.
- [12] S. Running, Q. Mu, M. Zhao, and A. Moreno, "MOD16A2 MODIS/Terra net evapotranspiration 8-day L4 global 500m SIN grid V061," *NASA EOSDIS Land Processes Distributed Active Archive Center*, 2021.
- [13] F. Zuze, "The economic valuation of Lake Chiuta wetland: A case study of Machinga district," Master's thesis, University of Malawi, Chancellor College, 2013.
- [14] S. Huang and S. Ontañón, "A closer look at invalid action masking in policy gradient algorithms," in *The International FLAIRS Conference Proceedings*, vol. 35, 2022.
- [15] A. Raffin, A. Hill, A. Gleave, A. Kanervisto, M. Ernestus, and N. Dornmann, "Stable-baselines3: Reliable reinforcement learning implementations," *Journal of Machine Learning Research*, vol. 22, no. 268, pp. 1–8, 2021.
- [16] J. Schulman, F. Wolski, P. Dhariwal, A. Radford, and O. Klimov, "Proximal policy optimization algorithms," *arXiv preprint arXiv:1707.06347*, 2017.